Lee, K. H., Kim, H. J., Song, Y., Efficient crosswell EM tomography for monitoring geological sequestration of $CO_2$.
International Symposium on the Fusion Technology of Geosystem Engineering, Rock Engineering and Geophysical Exploration
Seoul, Korea, Nov. 18-19, 2003

# Efficient crosswell EM tomography for monitoring geological sequestration of $CO_2$

Ki Ha Lee[1], Hee Joon Kim[2], Yoonho Song[3]
[1]Lawrence Berkeley National Laboratory, Berkeley, U.S.A., [2]Pukyong National University, Busan, Korea
[3]Korea Institute of Geoscience & Mineral Resources, Daejeon, Korea

Abstract: $CO_2$ sequestration in oil reservoirs can be one of the most effective strategies for long-term removal of greenhouse gas from atmosphere. This paper presents an advantage of the localized nonlinear approximation of integral equation solutions for inverting crosswell electromagnetic data, which are observed as a part of pilot project of $CO_2$ flooding at the Lost Hills oil field in central California, U. S. A. To monitor the migration of $CO_2$, we have used 2-D cylindrically symmetric and 2.5-D tomographic inversion methods. These two schemes produce nearly the same images if the borehole separation is large compared with the skin depth. However, since the borehole separation is much less than five skin depths in this $CO_2$ injection experiment, the 2.5-D model seems to be more reliable than the 2-D model. In fact, the pre-injection 2.5-D image is more successfully compared with induction logs observed in the two wells than the 2-D model. From the time-lapse crosswell imaging, we can confirm the replacement of brine with $CO_2$ makes a decrease of conductivity.

## 1. Introduction

Six years have passed since the Kyoto Protocol was adopted in December 1997, in which member countries agreed to reduce greenhouse gas emissions 5 % below 1990 levels by 2012. The burning of fossil fuels to supply the world's enormous requirement for energy has caused a significant increase in global atmospheric emissions of carbon dioxide ($CO_2$). $CO_2$ sequestration in geological formation is the most direct management strategy for long-term removal of $CO_2$ from atmosphere. This may be both cost effective and environmentally safe. An ideal site for such projects would be shallow brine aquifers (Mckenna et al., 2003) or oil reservoirs (Li, 2003).

If $CO_2$ is to be sequestered within the subsurface, a rigorous monitoring program is required to observe its movement during and after the injection process. Time-lapse three-dimensional (3-D) seismic methods have been developed by the petroleum industry to monitor the movement of hydrocarbon fluids within producing reservoirs to improve overall hydrocarbon recovery rates. While this technology is expected to form the foundation for most monitoring programs involving $CO_2$ storage in the future, it may be too expensive. High-resolution imaging of electrical conductivity has been the subject of many studies in crosswell tomography using electromagnetic (EM) fields (Zhou et al., 1993; Wilt et al., 1995; Alumbaugh and Morrison, 1995; Newman, 1995; Alumbaugh and Newman, 1997). The theoretical understanding and associated field practices for crosswell EM methods are relatively mature, but fast and stable inversion of crosswell EM data is still a challenging problem.

Since Raiche (1974) first formulated a 3-D volume integral equation (IE) method, many numerical solutions have been presented on this subject (Hohmann, 1988). The main advantage of IE method over the finite difference (FD) and/or finite-element (FE) methods is its greater suitability for inversion. For example, IE formulation readily contains a sensitivity matrix, which can be revised at each inversion iteration at little expense. With the FD or FE method, in contrast, the sensitivity matrix has to be recomputed at each iteration at a cost nearly equal to that of full forward modeling. The IE method, however, has to overcome a severe practical limitation imposed on the size of imaging domain for inversion purposes. In this direction, several approximate methods such as localized nonlinear (LN) approximation (Habashy et al., 1993) and quasi-linear approximation (Zhdanov and Fang, 1996) have been developed. Recently, the LN approximation for a cylindrically symmetric model was applied to inverting single- (Kim et al., 2003) and cross-hole (Kim et al., 2004) EM data.

In this paper an advantage of the LN approximation of IE solutions is further exploited for a monitoring program devoted to geological sequestration of $CO_2$. To do this, we prepare two crosswell imaging schemes: one employs a 2-D cylindrically symmetric model (Kim et al., 2004) and the other a 2.5-D model (Song et al., 2001). The 2-D scheme is quite fast but assumes an unrealistic geometry, while the 2.5-D method uses rather a reasonable geometry but is slow (but still much faster than a full 3-D one). We begin our discussion with the behavior of

injected $CO_2$ in the subsurface. We then compare the accuracy of LN approximation for 2-D and 2.5-D models. Finally, we present an example application to field data obtained as a part of pilot project of $CO_2$ flooding at the Lost Hills oil field in central California, U. S. A.

## 2. $CO_2$ lifecycle

Johnson et al. (2001) summarized the lifecycle of $CO_2$ injected in a shallow saline aquifer. The injection of $CO_2$ into sandstones saturated with brine will cause significant changes within the reservoir. Upon initial release into the formation, free $CO_2$ will displace brine whilst migrating upward through the reservoir due to buoyancy. The primary trapping mechanism of free $CO_2$ will be 'structural trapping' below an impermeable seal. After the $CO_2$ has been locked in the reservoir for a while, it will begin to dissolve into the brine ('solubility trapping'). This will cause $CO_2$ to descend in the reservoir because brine becomes heavier when saturated with $CO_2$. Repeated EM measurements may potentially detect dissolved $CO_2$ due to increased ion content in the formation water.

The dissolution of $CO_2$ into brine releases excess hydrogen and bicarbonate into the formation water. This reduces pH of the reservoir and the induced acidic conditions will dissolve susceptible minerals within the rock frame, causing porosity to increase slightly. The breakdown of these minerals will release metallic cations into the formation water such as calcium, magnesium and iron. These cations can then combine with free bicarbonate anions to form carbonate minerals such as calcite, dolomite or siderite. This process is referred to as 'mineral trapping' of $CO_2$. Long-term mineral trapping of $CO_2$ is the most secure form of trapping because the $CO_2$ is in its most dense form and it is immobilized. The continued development of carbonate minerals will reduce porosity and permeability within the formation and may cement the rock grains together.

## 3. $CO_2$ flooding

In contrast, Li (2003) reviewed $CO_2$ flooding at Weyburn Field in Saskatchewan, Canada. Oil recovery through $CO_2$ flooding has long been a popular technology in the petroleum industry. Miscible $CO_2$ flooding is a complex process. Compositionally, supercritical $CO_2$ and oil phases change with time, pressure, and position in the reservoir. It is important, therefore, to understand the mechanisms in which injected $CO_2$ may cause changes in the multiphase system, which will have effects on time-lapse seismic responses. The resistivity of $CO_2$ is known to be on the order of 100 Ω-m, much higher than that of brine. The critical point of $CO_2$ is known to be 7.4 MPa and 31°C.

When $CO_2$ first comes into contact with oil, it dissolves up to a certain mole fraction (approximately 66 %). The dissolved $CO_2$ swells the volume of oil phase. If higher mole fraction is added to oil, a $CO_2$ rich phase, made up of both $CO_2$ and vaporized hydrocarbons from oil, is formed to lower viscosity, making it more mobile and faster flowing than the oil-rich phase. If the pressure remains high, the $CO_2$ rich phase contacts more fresh oil and it dissolves to saturation until a minimum miscibility pressure is achieved. At this point, a miscible phase is formed where the $CO_2$ rich phase has vaporized enough hydrocarbons and the resulting fluid mixes with oil in all proportions. The mixed oil-$CO_2$ phase can flow more freely under low interfacial tension between the oil trapped in small capillaries in rocks and the injectant in an increased total volume, compared with the water phase. If the reservoir pressure is too low, however, the $CO_2$ rich phase becomes preferentially enriched with lighter components (such as methane) rather than intermediate hydrocarbons and thus dissolves less in the oil phase than the injected $CO_2$, leading to a poor recovery. As $CO_2$ viscosity is much lower than oil viscosity, the $CO_2$ rich phase will have a tendency to bypass oil by viscous fingering, thus reducing the areal conformance. Significant $CO_2$ breakthrough could occur in heterogeneous reservoir rocks before 5 % pore volume is injected. $CO_2$ also has a much higher solubility in water than hydrocarbons and can diffuse through the water phase to swell bypassed oil until the oil is mobile.

## 4. LN approximation

Assuming an $e^{+i\omega t}$ time dependency and neglecting displacement currents, an IE solution for the electric field $\mathbf{E}(\mathbf{r})$ at $\mathbf{r}$ can be written by (Hohmann, 1975)

$$\mathbf{E}(\mathbf{r}) = \mathbf{E}_b(\mathbf{r}) - i\omega\mu \int_V \underline{\underline{\mathbf{G}}}_E(\mathbf{r}-\mathbf{r}') \cdot \Delta\sigma(\mathbf{r}')\mathbf{E}(\mathbf{r}')dv', \tag{1}$$

where $\mathbf{E}_b(\mathbf{r})$ is the background electric field, $\mathbf{G}_E(\mathbf{r}\text{-}\mathbf{r}')$ the electric Green's tensor, $\sigma$ the electrical conductivity, $\omega$ the angular frequency, and $\mu$ the magnetic permeability. In equation (1), $\Delta\sigma(\mathbf{r}')$ inside the integral means the excess conductivity, $\sigma(\mathbf{r}') - \sigma_b$, and the term $\Delta\sigma\mathbf{E}$ is called the scattering current (Hohmann, 1975). Each vector component of the Green tensor $\mathbf{G}_E(\mathbf{r}\text{-}\mathbf{r}')$ is the vector electric field at $\mathbf{r}$ due to a point source at $\mathbf{r}'$ with its current density of $(-i\omega\mu)^{-1}$ A/m$^2$, polarized in $x$, $y$, and $z$, respectively. To obtain a numerical solution of equation (1), the anomalous body is first divided into a number of cubic cells, and a constant electric field is assigned to each cell (Hohmann, 1988). Once the electric fields $\mathbf{E}(\mathbf{r})$ in the inhomogeneity are obtained from equation (1), magnetic fields $\mathbf{H}(\mathbf{r})$ at observation points are given by

$$\mathbf{H}(\mathbf{r}) = \mathbf{H}_p(\mathbf{r}) - i\omega\mu_0 \int_V \underline{\underline{\mathbf{G}}}_H(\mathbf{r},\mathbf{r}')\Delta\sigma(\mathbf{r}')\cdot\mathbf{E}(\mathbf{r}')d\mathbf{r}', \tag{2}$$

where

$$\underline{\underline{\mathbf{G}}}_H(\mathbf{r},\mathbf{r}') = -\frac{\nabla\times\underline{\underline{\mathbf{G}}}_E(\mathbf{r},\mathbf{r}')}{i\omega\mu_0}, \tag{3}$$

is the magnetic Green's tensor.

Habashy et al. (1993) suggested a way to linearize equation (1) as

$$\mathbf{E}(\mathbf{r}) = \mathbf{E}_p(\mathbf{r}) - i\omega\mu_0\left[\int_V \underline{\underline{\mathbf{G}}}_E(\mathbf{r},\mathbf{r}')\Delta\sigma(\mathbf{r}')d\mathbf{r}'\right]\cdot\mathbf{E}(\mathbf{r}) - i\omega\mu_0\int_V \underline{\underline{\mathbf{G}}}_E(\mathbf{r},\mathbf{r}')\Delta\sigma(\mathbf{r}')\cdot[\mathbf{E}(\mathbf{r}') - \mathbf{E}(\mathbf{r})]d\mathbf{r}'. \tag{4}$$

If the third term on the right-hand side is small enough, then the electric field at any point in the inhomogeneity can be expressed as

$$\mathbf{E}(\mathbf{r}) \approx \underline{\underline{\Gamma}}(\mathbf{r})\cdot\mathbf{E}_p(\mathbf{r}), \tag{5}$$

where

$$\underline{\underline{\Gamma}}(\mathbf{r}) = \left[\underline{\underline{\mathbf{I}}} + i\omega\mu_0\int_V \underline{\underline{\mathbf{G}}}_E(\mathbf{r},\mathbf{r}')\Delta\sigma(\mathbf{r}')d\mathbf{r}'\right]^{-1}, \tag{6}$$

is the 3 by 3 depolarization tensor introduced by Habashy et al. (1993), and $\underline{\underline{\mathbf{I}}}$ is the identity tensor.

The complexity associated with a full 3-D problem can be greatly reduced for a model whose conductivity is 2-D cylindrically symmetric in the vicinity of a borehole. In order to preserve the cylindrical symmetry in the resultant EM fields, a horizontal loop current or a vertical magnetic dipole may be considered as a source in the borehole. When the problem is formulated using an azimuthal electric field $E_\varphi$, which is scalar, the resultant IE solution is (e.g., Kim et al., 2003)

$$E_\varphi(\rho,z) = E_{\varphi b}(\rho,z) - 2\pi i\omega\mu\iint_{\rho z} G_E(\rho,\rho';z-z')\Delta\sigma(\rho',z')E_\varphi(\rho',z')\rho'\,d\rho'\,dz'. \tag{7}$$

The Green's function, which is also scalar, is given in the form of a Hankel transform as (Ward and Hohmann, 1988, p. 219)

$$G_E(\rho,\rho';z-z') = -\frac{1}{4\pi}\int_0^\infty \frac{e^{-u_b|z-z'|}}{u_b}\lambda J_1(\lambda\rho)J_1(\lambda\rho')d\lambda, \tag{8}$$

where $u_b = (\lambda^2 + i\omega\mu\sigma_b)^{1/2}$ is the vertical wave number and $J_1$ is the Bessel function of order 1. In contrast, for a 2.5-D model (2-D geometry with strike $y$-axis with a point source), rewriting equation (1) in the wavenumber domain with respect to $y$-axis yields (Song et al., 2001)

$$\mathbf{E}(\mathbf{r}) = \mathbf{E}_b(\mathbf{r}) - \frac{i\omega\mu}{2\pi}\int_{-\infty}^{\infty}\left[\int_S \tilde{\underline{\mathbf{G}}}_E(x-x', k_y, z-z')\cdot\Delta\sigma(x',z')\tilde{\mathbf{E}}(x', k_y, z')dx'dz'\right]e^{ik_y y}dk_y , \qquad (9)$$

where the '~' sign means the Fourier transformed quantity with respect to $y$ and $k_y$ is the wavenumber. Song et al. (2001) developed a 2.5-D inversion method using the LN approximation to equation (9) for both forward and sensitivity calculations, while Kim et al. (2004) used the LN approximation to equation (7) for their rapid 2-D inversion scheme.

## 5. Crosswell tomography

The 2-D and 2.5-D inversion algorithms have been tested using a set of crosswell EM data collected as a part of water flood monitoring at the Lost Hills oil field in central California (Wilt et al., 2001). Two fiberglass cased wells were installed at the southern margin of the oil field for the monitoring and the separation between these two observation wells was 82 m. Although EM data for the pre- and post-injection of water are available, we analyze only the pre-injection EM data ($H_z$ fields due to $M_z$ sources). The operating frequency was 1,000 Hz.

A 2-D inversion result is shown in Figure 1 along with a 2.5-D inversion result. For the sake of comparison we use no geological information to invert the crosswell EM data except for the smoothness constraint. The cell size for these images is 5 × 5 m. Initial model used is 1.4 Ω-m uniform whole space and after 5 iterations the rms misfit is reduced to below 10 %. Both methods give similar images in spite of different model dimensions. The resistive (1.5 – 2 Ω-m) zone shallower than about 760 m is considered as the chief oil bearing zone at the field (Wilt et al., 2001).

Alumbaugh and Morrison (1995) showed the general applicability of the cylindrically symmetric geometry by comparing the 2-D sensitivity functions to those produced by a 2.5-D model. For borehole separations greater than five skin depths ($a/\delta > 5$, where $a$ is the borehole separation and $\delta$ is the skin depth), it is demonstrated that the measurements and thus the images are not affected by the geometry of the conductive zone outside of the interwell plane. As $a/\delta$ becomes much smaller than 5, however, artifacts are produced in the images which will lead to faulty interpretations. In our case, $a/\delta \approx 4.5$ because the skin depth is about 19 m. So the reconstructed images may have few artifacts and the approximation of 2-D cylindrical geometry can provide similar results to those other schemes at much less computational cost.

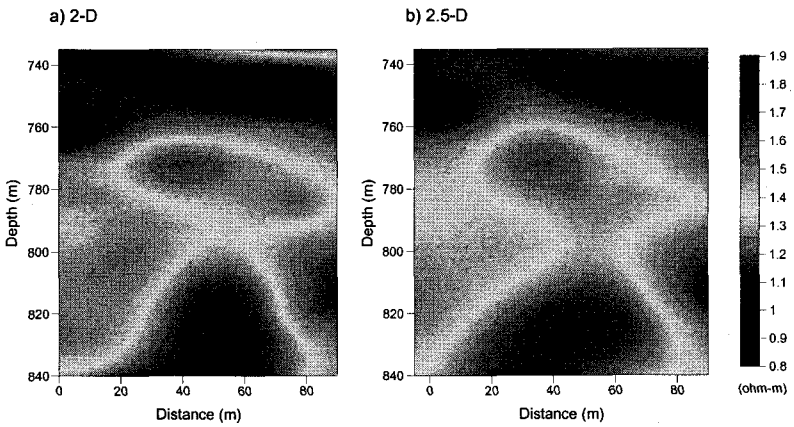


Figure 1. Comparison of resistivity images derived from the 2-D (a) and 2.5-D (b) inversion of crosswell EM data collected at the Lost Hills oil field in central California. The pixel size for these images is 5 × 5 m and the initial model is a homogeneous whole space of 1.4 Ω-m.

Next, the two inversion algorithms have been applied to a set of field crosswell EM data provided by Chevron as a part of the Lost Hills $CO_2$ pilot project in southern California (Wilt, 2002). The separation between two observation wells is 24.536 m and $CO_2$ injection well is near the center of the section defined by the two observation wells. Although both EM and seismic data for the pre- and post-injection of $CO_2$ are available, we analyzed only EM data. The operating frequency was 759 Hz.

Figure 2 shows time-lapse resistivity images derived from the crosswell EM data using the 2-D cylindrically symmetric model. The $CO_2$ injection into a reservoir of oil/brine mixture results in changes in conductivity, which can be indirectly interpreted as the displacement of brine with injected $CO_2$. The replacement of water with $CO_2$ makes a decrease of conductivity. Figure 2 shows a significant change in resistivity distribution; the resistivity before the $CO_2$ injection ranges from 1.7 Ω-m to 3.2 Ω-m, while that after the injection has the range of 1.6 – 4.5 Ω-m. This increase of resistivity suggests a clear effect of the injected $CO_2$ migration. Unfortunately, because the borehole separation is not far enough compared with the skin depth ($a/\delta \approx 0.8$), the cylindrical sensitivity can be relatively high in a large area outside of the interwell plane (Alumbaugh and Morrison, 1995). Reconstructed images thus may have artifacts produced by the geometry of conductive zone outside of the interwell region.

In contrast, Figure 3 shows time-lapse resistivity images obtained using the 2.5-D model. From this illustration, we can also find a significant increase in resistivity distribution; the resistivity before the $CO_2$ injection ranges from 1.5 Ω-m to 3.9 Ω-m, while that after the injection has the range of 1.3 – 4.9 Ω-m. Comparing Figure 3 with Figure 2, however, one can find the resistivity images are slightly different from each other. Since $a/\delta$ is much less than 5, the 2.5-D model seems to be more reliable than the 2-D model in this $CO_2$ injection experiment. In fact, the pre-injection 2.5-D image is successfully compared with induction logs observed in the two wells as shown in Figure 4, while the consistency between the pre-injection 2-D image (left of Figure 2) and the induction logs is not so high.

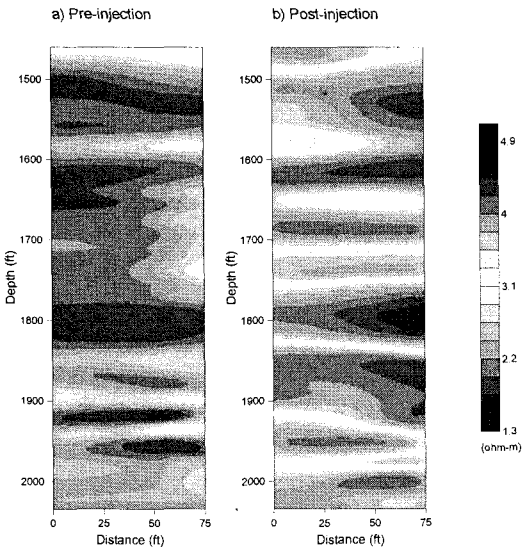


Figure 2. Time-lapse CO2 injection images derived from the 2-D cylindrically symmetric inversion of crosswell EM data collected at the Lost Hills oil field in central California. The pixel size for these images is 2.5 × 2.5 m. The images are horizontally elongated by a fact of 2.3.

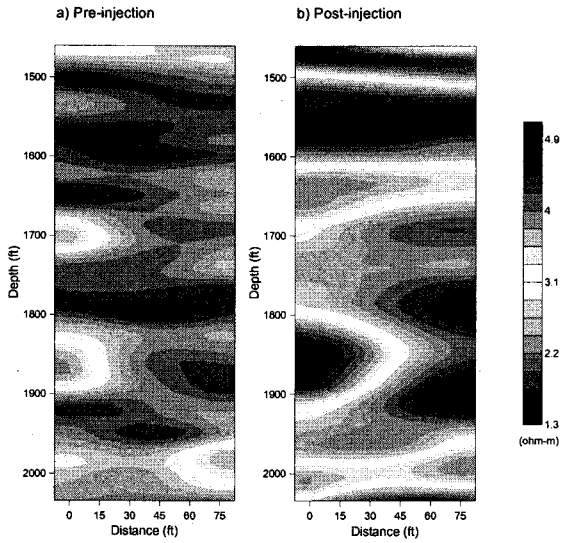


Figure 3. Time-lapse CO2 injection images derived from the 2.5-D inversion of crosswell EM data collected at the Lost Hills oil field in central California. The pixel size for these images is 2.5 × 2.5 m. The images are horizontally elongated by a fact of 2.3.

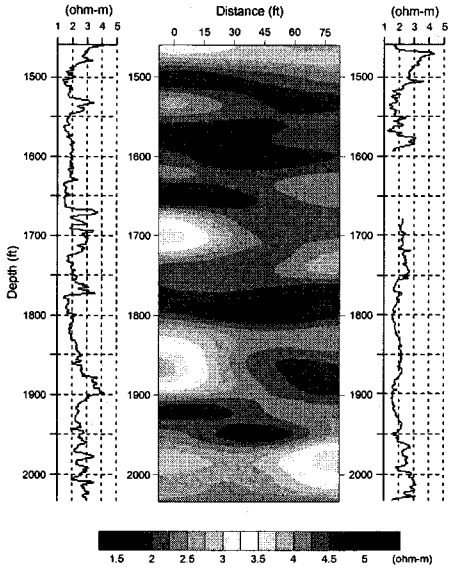


Figure 4. Pre-injection resistivity image derived from the 2.5-D inversion with induction resistivity logs.

## 6. Conclusions

In this paper we exploit an advantage of the LN approximation of IE solutions for a monitoring program devoted to geological sequestration of $CO_2$. To do this, we prepare two crosswell tomography schemes: one uses the 2-D cylindrically symmetric model and the other the 2.5-D model. The 2-D scheme is quite fast but assumes an unrealistic geometry, while the 2.5-D method uses rather a reasonable geometry but is slow (but still much faster than a full 3-D one). The general applicability of these models is tested using field crosswell EM data obtained as a part of pilot project of $CO_2$ flooding at the Lost Hills oil field in central California, U. S. A. The $CO_2$ injection into

a reservoir of oil/brine mixture results in changes in conductivity, which can be indirectly interpreted as the displacement of brine with injected $CO_2$. From the time-lapse crosswell EM imaging, we can confirm the replacement of brine with $CO_2$ makes a decrease of conductivity. Since the borehole separation is much less than five skin depths, the 2.5-D model seems to be more reliable than the 2-D model in this $CO_2$ injection experiment. In fact, the pre-injection 2.5-D image is successfully compared with induction logs observed in the two wells.

## Acknowledgements

This work was partially supported by the Assistant Secretary for Energy Efficiency and Renewable Energy, Office of Wind and Geothermal Technologies of the U.S. Department of Energy under Contract No. DE-AC03-76SF00098. The third author's (Y. Song) work was supported by the Korean Ministry of Science and Technology through National Research Lab. Funding.

## References

Alumbaugh, D.L. and Morrison, H.F., 1995, Theoretical and practical considerations for crosswell electromagnetic tomography assuming a cylindrical geometry: *Geophysics*, **60**, 846-870.

Alumbaugh, D.L., and Newman, G.A., 1997, Three-dimensional massively parallel electromagnetic inversion— II. Analysis of crosswell electromagnetic experiment: *Geophys. J. Int.*, **128**, 355-363.

Habashy, T.M., Groom, R.M., and Spies, B.R., 1993, Beyond the Born and Rytov approximations: a nonlinear approach to electromagnetic scattering: *J. Geophys. Res.*, **98**, 1795-1775.

Hohmann, G.W., 1975, Three-dimensional induced polarization and EM modeling: *Geophysics*, **40**, 309-324.

Hohmann, G.W., 1988, Numerical modeling for electromagnetic methods of geophysics, *in* Nabighian, M.N., Ed., Electromagnetic Methods in Applied Geophysics, Vol. 1, Soc. Expl. Geophys., 313-363.

Johnson, J.W., Nitao, J.J., Steefel, C.I., and Knauss, K.G., 2001, Reactive transport modeling of geologic $CO_2$ sequestration in saline aquifers: the influence of intra-aquifer shales and the relative effectiveness of structural, solubility and mineral trapping during prograde and retrograde sequestration: Proc. 1st Nat. Conf. On Carbon Sequestration, Washington, D.C.

Kim, H.J., Lee, K.H., and Wilt, M., 2003, A fast inversion method for interpreting borehole electromagnetic data, *Earth Planets Space*, **55**, 249-254.

Kim, H.J., Song, Y., Lee, K.H., and Wilt, M., 2004, Efficient crosswell EM tomography using localized nonlinear approximation, *Expl. Geophys.*, **57**. (in press)

Li, G., 2003, 4D seismic monitoring of $CO_2$ flood in a thin fractured carbonate reservoir, *Leading Edge*, **22**, 690-695.

McKenna, J., Gurevich, B., Urosevic, M., and Evans, B., 2003, Estimating bulk and shear moduli for shallow saline aquifers undergoing $CO_2$ injection, Proc. 6th SEGJ Int. Symp., 490-497.

Newman, G.A., 1995, Crosswell electromagnetic inversion using integral and differential equations: *Geophysics*, **60**, 899-911.

Raiche, A.P., 1974, An integral equation approach to 3D modeling: *Geophys. J. Roy. astr. Soc.*, **36**, 363-376.

Song, Y., Kim, J.-H., and Chung, S.-H., 2001, An efficient 2.5-D inversion of loop-loop EM data, Proc. 5th SEGJ Int. Symp., 153-160.

Ward, S.H., and Hohmann, G.W., 1988, Electromagnetic theory for geophysical applications, *in* Nabighian, M.N., Ed., Electromagnetic Methods in Applied Geophysics, Vol. 1, Soc. Expl. Geophys., 131-311.

Wilt, M.J., Alumbaugh, D.L., Morrison, H.F., Becker, A., Lee, K.H., and Deszcz-Pan, M., 1995, Crosshole electromagnetic tomography: System design considerations and field results: *Geophysics*, **60**, 871-885.

Wilt, M.J., Zhang, P., Osato, K., and Tsuneyama, F., 2001, Crosswell EM studies at the Ellis Lease, Lost Hills California, Proc. 5th SEGJ Int. Symp., 243-250.

Wilt, M.J., Mallan, R., Kasameyer, P., and Kirkkendall, B., 2002, Extended 3D induction logging for geothermal resource assessment: Field results with the Geo-BILT system, Proc. 27th Workshop on Geothermal Reservoir Eng., Stanford Univ., SGP-TR-171.

Zhdanov, M.S., and Fang, S., 1996, Quasi-linear approximation in 3-D EM modeling: *Geophysics*, **61**, 646-665.

Zhou, Q., Becker, A., and Morrison, H.F., 1993, Audio-frequency electromagnetic tomography in 2-D: *Geophysics*, **58**, 482-495.